Surface Potential and Interfacial Water Order at the Amorphous TiO_2 Nanoparticle/Aqueous Interface

Marie Bischoff[1], Denys Biriukov[2], Milan Předota[2], Sylvie Roke[1*] and Arianna Marchioro[1*]

[1] *Laboratory for fundamental BioPhotonics (LBP), Institute of Bioengineering (IBI), and Institute of Materials Science (IMX), School of Engineering (STI), École polytechnique fédérale de Lausanne (EPFL), CH-1015 Lausanne, Switzerland.*

[*] *E-mail : arianna.marchioro@epfl.ch, sylvie.roke@epfl.ch*

[2] *Institute of Physics, Faculty of Science, University of South Bohemia, 370 05 České Budějovice, Czech Republic*

Supplementary Information

AR-SHS model and theory – relevant constants, analytical expressions and assumptions

Table S1: Constants, geometrical form factor functions and scattering vector used for calculating the scattered intensity from spherical particles (equations 4 and 5).

Geometrical form factors
$F_1(qR) = 2\pi R^2 i \left(\frac{\sin(qR)}{(qR)^2} - \frac{\cos(qR)}{qR} \right)$
$F_2(qR) = 4\pi R^2 i \left(3\frac{\sin(qR)}{(qR)^4} - 3\frac{\cos(qR)}{(qR)^3} - \frac{\sin(qR)}{(qR)^2} \right)$
$F_3(\kappa R, qR) = 2\pi R^2 i \frac{qR\cos(qR)+\kappa R\sin(qR)}{(qR)^2+(\kappa R)^2}$
Scattering vector
$\mathbf{q} \equiv \mathbf{k_0} - 2\mathbf{k_1}, \;\; q = \left\| \frac{4\pi n_{\mathrm{H_2O}}}{\lambda_{\mathrm{SH}}} \sin\frac{\theta}{2} \right\|$
Constants
$\mu_{DC} = 8.97 \cdot 10^{-30}\,\mathrm{Cm}$
$\bar{\beta}^{(2)} = 3.09 \cdot 10^{-52}\,\mathrm{C^3 m^3 J^{-2}}$
$\bar{\beta}^{(3)} = 4.86 \cdot 10^{-62}\,\mathrm{C^4 m^4 J^{-3}}$

The geometrical form factor functions for spheres, as they are shown in Table S1 can also be found in Refs.[1,2] They depend on the radius of the particles R and the scattering vector $|\mathbf{q}| = q$. The third form factor also depends on the inverse Debye length κ and therefore the ionic strength of the solvent. The Debye length is defined as $\kappa^{-1} = \sqrt{(\varepsilon_0 \varepsilon_r k_B T)/(2000 e^2 z^2 N_{Av} c)}$ and takes into account the vacuum and relative permittivity ε_0 and ε_r respectively, the Boltzmann constant k_B, the temperature T, the elementary charge e, the valency z, Avogadro's number N_{Av} and the ionic concentration c. The constants used to calculate the scattered intensity from spherical particles in equations 4 and 5 are the dipole moment of water μ_{DC}, and the hyperpolarizability tensor elements of water $\overline{\beta}^{(2)}$ and $\overline{\beta}^{(3)}$. The values of the hyperpolarizability tensor elements were computed from an ab-initio model (using 1064 nm incoming light, Table 4, Model IIIa, of Ref. [3]). Although there are 3 $\beta^{(2)}$ or 6 $\beta^{(3)}$ nonzero hyperpolarizability tensor elements for a single water molecule, a single mean value can be obtained by averaging over many water molecules in an isotropic liquid, here indicated as $\overline{\beta}^{(2)}$ and $\overline{\beta}^{(3)}$.

Table S2 summarizes some important equalities as well as the surface and effective particle susceptibility elements needed to compute the second harmonic scattering intensity from spherical particles in solution. The non-zero second- and third-order susceptibility elements $\chi_{s,1}^{(2)}$, $\chi_{s,2}^{(2)}$ and $\chi_2^{(3)'}$ are corrected for changes in the refractive index occurring at the particle/liquid interface following Refs.[4,5] so that dispersion can be neglected. It was found in previous studies that a linear correction term as proposed by Dadap et al.[5] is sufficient to correct for the changes in the orthogonal coordinate of the electromagnetic field when it crosses the particle/liquid interface.[6] The corrected susceptibility elements $\chi_{s,1}^{(2)''}$, $\chi_{s,2}^{(2)''}$ and $\chi_2^{(3)''}$ are than inserted into the analytical expressions for the non-zero effective particle susceptibility elements $\Gamma_1^{(2)}$, $\Gamma_2^{(2)}$ and $\Gamma_2^{(3)'}$ needed to calculate the scattering intensity in equations 4 and 5. The effective particle susceptibilities represent the combined symmetry of the incoming electromagnetic fields, the geometry of the scatterers (here: spherical), the interfacial structure and the electrostatic field in the aqueous phase. Note that the scattering intensity equations 4 and 5 are only valid under the assumption that dispersion from the difference in the refractive indices of the particles (n_p) and the

Table S2: Effective particle susceptibilities and surface susceptibility elements and their equalities used for computing the scattering intensity from spherical particles (equations 4 and 5). ⊥ refers to the direction perpendicular to the particle surface and ∥ to the direction parallel to the particle surface. The second- and third-order susceptibility elements are corrected for changes in the refractive index occurring at the particle/liquid interface following Ref. [4,5] so that dispersion can be neglected.

Second-order surface susceptibilities and their equalities
$\chi_{s,1}^{(2)} = \chi_{s,\perp\perp\perp}^{(2)} - \chi_{s,\parallel\parallel\perp}^{(2)} - \chi_{s,\parallel\perp\parallel}^{(2)} - \chi_{s,\perp\parallel\parallel}^{(2)},\ \chi_{s,1}^{(2)} \to 0$
$\chi_{s,2}^{(2)} = \chi_{s,\parallel\parallel\perp}^{(2)},\ \chi_{s,2}^{(2)} = \chi_{s,3}^{(2)} = \chi_{s,4}^{(2)}$
Effective third-order susceptibilities and their equalities
$\chi_1^{(3)'} = \chi_{\perp\perp\perp,\perp}^{(3)'} - \chi_{\parallel\parallel\perp,\perp}^{(3)'} - \chi_{\parallel\perp\parallel,\perp}^{(3)'} - \chi_{\perp\parallel\parallel,\perp}^{(3)'},\quad \chi_1^{(3)'} = 0$
$\chi_2^{(3)'} = \frac{N_b}{\epsilon_0}\left(\bar{\beta}^{(3)} + \frac{\bar{\beta}^{(2)}\mu_{DC}}{3k_BT}\right) = 10.3 \cdot 10^{-22}\,\mathrm{m^2V^{-2}},\quad \chi_2^{(3)'} = \chi_3^{(3)'} = \chi_4^{(3)'}$
Corrected surface- and effective third-order susceptibilities
$\chi_{s,1}^{(2)''} = 27\eta\frac{\left(\chi_{s,1}^{(2)}\eta^2 + 3\chi_{s,2}^{(2)}(\eta^2-1)\right)}{(2+\eta)^3},\quad \eta = \left(\frac{n_p}{n_{\mathrm{H_2O}}}\right)^2$
$\chi_{s,2}^{(2)''} = 27\eta\frac{\chi_{s,2}^{(2)}}{(2+\eta)^3}$
$\chi_2^{(3)''} = 27\eta\frac{\chi_2^{(3)'}}{(2+\eta)^3}$
Effective particle susceptibilities
$\Gamma_1^{(2)} = (2F_1(qR) - 5F_2(qR))\,\chi_{s,1}^{(2)''}$
$\Gamma_2^{(2)} = F_2(qR)\chi_{s,1}^{(2)''} + 2F_1(qR)\chi_{s,2}^{(2)''}$
$\Gamma_2^{(3)'} = 2\chi_2^{(3)''}\Phi_0\,(F_1(qR) + F_3(qR,\kappa R))$

liquid (n_{H2O}) can be neglected and that no multiple scattering events occur. Dynamic light scattering experiments and second harmonic scattering experiments as a function of particle concentration (not shown here) proved that the
intensity scales linearly with the particle concentration ensuring that those assumptions hold. The expressions for the surface and effective particle susceptibilities, presented in Table S2, are derived using five commonly used assumptions [7] that are related to the optical properties of isotropic materials and their behavior in nonresonant second harmonic scattering experiments:

1. The liquids can be considered as spatially isotropic reducing the number of possible 81 elements (considering a loss-less medium and that the electric

fields are real) of the $\chi^{(3)'}$ and $\Gamma^{(3)'}$ tensors to only 4 remaining non-zero elements (Ref. [7] page 53).

2. Applying the assumptions that the material is loss-less and that the electric fields are real reduces the amount of possible elements for $\chi^{(2)}$ and $\Gamma^{(2)}$ to 27. As the particle interface can be considered as isotropic in the interfacial plane, meaning that tangential coordinates are interchangeable, the number of non-zero elements reduces to 4 elements for $\chi_s^{(2)}$ and $\Gamma^{(2)}$.
3. Assuming the absence of dispersion due to the probing being off-resonant, three of the four tensor elements of $\chi_s^{(2)}$ ($\Gamma^{(2)}$) and $\chi^{(3)'}$ ($\Gamma^{(3)'}$) are equal to one another ($\chi_{s,2}^{(2)} = \chi_{s,3}^{(2)} = \chi_{s,4}^{(2)}$ and $\chi_2^{(3)'} = \chi_3^{(3)'} = \chi_4^{(3)'}$) so that only two independent tensor elements remain. Those are $\chi_{s,1}^{(2)}$ and $\chi_{s,2}^{(2)}$, and $\chi_1^{(3)'}$ and $\chi_2^{(3)'}$ respectively. This assumption was verified by confirming that the polarization combinations PSS and SPS (or SSP) generate the same SHS response within experimental uncertainty. Mind that SPS and SSP are the same in SHS as we are using a single incoming frequency $\omega_1 = \omega_2 = \omega$ which makes the last two indices interchangeable.
4. Additionally, the element $\chi_1^{(3)'}$ is equal to zero due to symmetry properties of the third-order susceptibility tensor of an isotropic medium (namely $\chi_1^{(3)'} = \chi_{\perp\perp\perp,\perp}^{(3)'} - \chi_{\|\|\perp,\perp}^{(3)'} - \chi_{\|\perp\|,\perp}^{(3)'} - \chi_{\perp\|\|,\perp}^{(3)'} = 0$).[8,9] Thus also $\Gamma_1^{(3)'} = 0$ (Ref. [2]).
5. We finally assume that $\chi_{s,1}^{(2)}$ = 0, which is the case for a broad orientational distribution of water molecules at the interface. See Ref. [9] for details.

Experimental parameters used for fitting the AR-SHS patterns

Table S3: Parameters used for fitting the normalized second harmonic scattering patterns applying the AR-SHS model. These parameters are common to all the TiO_2 sets of data presented and fitted.

Second harmonic wavelength λ [nm]	515
Refractive index n_{H_2O} (@ 515 nm)	1.33
Refractive index n_{TiO_2} (@ 515 nm)	2.61
Temperature [°C]	23
Number of particles	$4.26 \cdot 10^{11}$

Table S4: Parameters used for fitting the normalized second harmonic scattering patterns applying the AR-SHS model. These parameters are common to all sets of SiO_2 data presented and fitted.

Second harmonic wavelength λ [nm]	515
Refractive index n_{H_2O} (@ 515 nm)	1.33
Refractive index n_{SiO_2} (@ 515 nm)	1.46
Temperature [°C]	23
Number of particles	$2.91 \cdot 10^{11}$

Table S5: Parameters used for fitting the normalized second harmonic scattering patterns of 100 nm amorphous TiO_2 particles applying the AR-SHS model. The ionic strength is determined via conductivity as described in the Materials and Methods section. The values presented are specifically used for fitting the NaCl concentration series.

added NaCl [μM]	0	10	50	100	300
Radius [nm]	59	60	60	60	59
Ionic strength [μM]	40.4	46.5	91.2	134.7	311. 0

Table S6: Parameters used for fitting the normalized second harmonic scattering patterns of 100 nm amorphous TiO_2 particles applying the AR-SHS model. The ionic strength is determined via conductivity as described in the Materials and Methods section. The values presented are specifically used for fitting the pH series.

pH	7	9.5	10.7
Radius [nm]	63	63	59
Ionic Strength [μM]	39.1	98.0	569.7

Table S7: Parameters used for fitting the normalized second harmonic scattering patterns of 100 nm SiO_2 particles applying the AR-SHS model. The ionic strength is determined via conductivity as described in the Materials and Methods section. The values presented are specifically used for fitting the NaCl concentration series.

added NaCl [μM]	0	10	50	100	300	600
Radius [nm]	65	64	62	61	60	58
Ionic strength [μM]	13.0	23.0	57.5	96.6	288. 0	561. 0

Surface charge densities and deprotonation

From surface charge density values found in the literature[10–13] that were measured by potentiometric titration, we calculated the percentage of deprotonation at pH 7 using an initial density of 4.8 OH/nm^2 as determined for the hydroxylated surface of P25 TiO_2 particles (Degussa) taken from Ref. [14] The radius of the particles was taken as 60 nm, which is close to what was measured in our dynamic light scattering experiments for amorphous TiO_2 particles. We obtain a deprotonation of 1% using the reported surface charge densities of - 0.00763 C/m^2 for 21 nm diameter P25 TiO_2 particles (Degussa) at pH 7.10 by Holmberg et al.,[10] and - 0.00833 C/m^2 for ≈ 72 nm diameter rutile TiO_2 particles (CL/D 528 Tioxide International Limited) at pH 7.13 by Yates.[11] Values up to - 0.06417 C/m^2 have been reported by Machesky et al.[12] for ≈ 83 nm diameter rutile TiO_2 particles (Tioxide Specialities Ltd.) at pH 7.02, which correspond to deprotonation values of 8%. Similar values were reported by Akratopulu et al.[13] for 30 nm diameter P25 TiO_2 particles (Degussa) at pH 6.93 who obtained a surface charge density of - 0.05074 C/m^2 which corresponds to a deprotonation of 7%.

Calculating the percentage of deprotonation in the same way for pH 9.5 by using the reported surface charge densities of - 0.06250 C/m^2 for 21 nm diameter P25 TiO_2 particles (Degussa) at pH 9.3 (Holmberg et al.)[10] and - 0.07431 C/m^2 for ≈ 72 nm rutile TiO_2 particles synthesized at pH 9.6 (Yates)[11] we obtain a deprotonation of 8-10%. Higher deprotonation values, up to 35% are calculated using a surface charge density of - 0.27644 C/m^2 reported at pH 9.4 by Akratopulu et al.[13] for 30 nm diameter P25 TiO_2 particles. Machesky et al.[12] found similar values for the surface charge density of ≈ 83 nm diameter rutile TiO_2 particles at pH 9.63 (- 0.22686 C/m^2) translating into 30% deprotonation. Given the fact that the measurements in Holmberg et al.,[10] Yates,[11] Machesky et al.[12] and Akratopulo et al.[13] were performed at higher ionic strength of 0.1 M $NaNO_3$, 1 mM KNO_3, 0.03 M NaCl and 0.1 M KNO_3, respectively, the calculated deprotonation values can be regarded as an upper limit for the real deprotonation that we expect for our amorphous TiO_2 particles in the lower ionic strength region.

AR-SHS below pH 7

For 4 < pH < 7, where HCl is added to the TiO_2 dispersion, but the particle surface remains negatively charged (as the isoelectric point is at pH = 4, and here as first approximation the isoelectric point can be considered equal to the point of zero charge), no SHS patterns could be obtained due to particle aggregation that occurs close to the isoelectric point. The acidic pH range below the isoelectric point, where the surface is positively charged, was not experimentally accessible: With addition of HCl, the particles were unstable between $3 \leq pH \leq 4$ and the signal-to-noise ratio of the SHS patterns was too low for pH < 3.

AR-SHS patterns of 100 nm diameter SiO_2 particles as a function of NaCl concentration

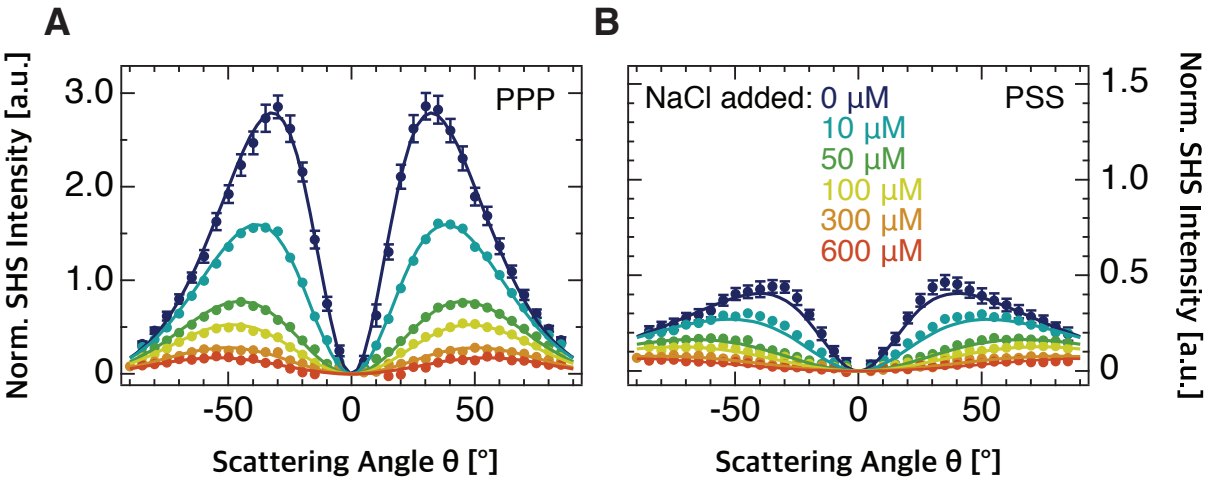

Figure S1: AR-SHS patterns of 100 nm diameter SiO_2 particles as a function of ionic strength in PPP (**A**) and PSS (**B**) polarization combination. Plain data points of different colors represent different salt concentrations of the aqueous environment. The ionic strength was adjusted through NaCl addition. The particle density was kept constant for each sample and equal to $2.9 \cdot 10^{11}$ particles/ml. All measurements were performed at T = 296.15 K. Solid lines represent the fits to the corresponding data points using the AR-SHS model. A summary of all the parameters used for the fits can be found in Tables S4 and S7.

References

(1) de Beer, A. G. F.; Roke, S. Obtaining Molecular Orientation from Second Harmonic and Sum Frequency Scattering Experiments in Water: Angular Distribution and Polarization Dependence. *J. Chem. Phys.* **2010**, *132*, 234702.

(2) Gonella, G.; Lütgebaucks, C.; de Beer, A. G. F.; Roke, S. Second Harmonic and Sum-Frequency Generation from Aqueous Interfaces Is Modulated by Interference. *J. Phys. Chem. C* **2016**, *120*, 9165-9173.

(3) Gubskaya, A. V.; Kusalik, P. G. The Multipole Polarizabilities and Hyperpolarizabilities of the Water Molecule in Liquid State: An Ab Initio Study. *Mol. Phys.* **2001**, *99*, 1107-1120.

(4) Dadap, J. I. Second-Harmonic Rayleigh Scattering from a Sphere of Centrosymmetric Material. *Phys. Rev. Lett.* **1999**, *83*, 4045–4048.

(5) Dadap, J. I.; Shan, J.; Heinz, T. F. Theory of Optical Second-Harmonic Generation from a Sphere of Centrosymmetric Material: Small-Particle Limit. *J. Opt. Soc. Am. B* **2004**, *21*, 1328.

(6) Lütgebaucks, C.; Gonella, G.; Roke, S. Optical Label-Free and Model-Free Probe of the Surface Potential of Nanoscale and Microscopic Objects in Aqueous Solution. *Phys. Rev. B* **2016**, *94*, 195410.

(7) Boyd, R. *Nonlinear Optics*, 3rd ed.; Academic Press, Elsevier Science: Amsterdam, 2008.

(8) de Beer, A.; Kramer Campen, R.; Roke, S. Separating Surface Structure and Surface Change with Second-Harmonic and Sum-Frequency Scattering. *Phys. Rev. B* **2010**, *82*, 235431.

(9) de Beer, A. G. F.; Roke, S. What Interactions Can Distort the Orientational Distribution of Interfacial Water Molecules as Probed by Second Harmonic and Sum Frequency Generation? *J. Chem. Phys.* **2016**, *145*, 044705.

(10) Holmberg, J. P.; Ahlberg, E.; Bergenholtz, J.; Hassellöv, M.; Abbas, Z. Surface Charge and Interfacial Potential of Titanium Dioxide Nanoparticles: Experimental and Theoretical Investigations. *J. Colloid Interface Sci.* **2013**, *407*, 168–176.

(11) Yates, D. E. *The Structure of the Oxide/Aqueous Electrolyte Interface*; PhD Dissertation. Faculty of Science. Chemistry. University Melbourne, 1975.

(12) Machesky, M. L.; Wesolowski, D. J.; Palmer, D. A.; Ichiro-Hayashi, K. Potentiometric Titrations of Rutile Suspensions to 250°C. *J. Colloid Interface Sci.* **1998**, *200*, 298–309.

(13) Akratopulu, K. Ch.; Kordulis, C.; Lycourghiotis, A. Effect of Temperature on the Point of Zero Charge and Surface Charge of TiO_2. *J. Chem. Soc. Faraday Trans.* **1990**, *86*, 3437.

(14) Mueller, R.; Kammler, H. K.; Wegner, K.; Pratsinis, S. E. OH Surface Density of SiO_2 and TiO_2 by Thermogravimetric Analysis. *Langmuir* **2003**, *19*, 160–165.